Role of Balanced Charge Carrier Transport in Low Band Gap polymer

Kotlarski, Jan D.; Moet, Date J. D.; Blom, Paul W. M.

Published in:
Journal of Polymer Science. Part B: Polymer Physics

DOI:
10.1002/polb.22243

Publication date:
2011

Role of Balanced Charge Carrier Transport in Low Band Gap polymer:fullerene Bulk Heterojunction Solar Cells

Jan D. Kotlarski,[1] Date J. D. Moet,[1] Paul W. M. Blom[1,2]

[1]Molecular Electronics, Zernike Institute for Advanced Materials, University of Groningen, Nijenborgh 4, 9747 AG Groningen, The Netherlands

[2]Holst Centre, High Tech Campus 31, 5605 KN Eindhoven, The Netherlands

Correspondence to: P. W. M. Blom (E-mail: p.w.m.blom@rug.nl)

Received 14 January 2011; revised 1 March 2011; accepted 1 March 2011; published online 1 April 2011
DOI: 10.1002/polb.22243

ABSTRACT: Lowering of the optical band gap of conjugated polymers in bulk heterojunction solar cells not only leads to an increased absorption but also to an increase of the optimal active layer thickness due to interference effects at longer wavelengths. The increased carrier densities due to the enhanced absorption and thicker active layers make low band gap solar cells more sensitive to formation of space charges and recombination. By systematically red shifting the optical parameters of poly[2-methoxy-5-(3′,7′-dimethyloctyloxy)-*p*-phenylenevinylene] and 6,6-phenyl C_{61}-butyric acid methyl ester, we simulate the effect of a reduced band gap on the solar cell efficiencies. We show that especially the fill factor of low band gap cells is very sensitive to the balance of the charge transport. For a low band gap cell with an active layer thickness of 250 nm, the fill factor of 50% for balanced transport is reduced to less than 40% by an imbalance of only one order of magnitude. © 2011 Wiley Periodicals, Inc. J Polym Sci Part B: Polym Phys 49: 708–711, 2011

KEYWORDS: charge transport; conducting polymers; computer modeling

The efficiency of organic polymer:fullerene bulk heterojunction solar cell performance has been steadily increasing in the last years, going from 2.5% efficiency in 2001[1] to 3.5% in 2003,[2] up to 5.5% in 2007,[3,4] and recently an efficiency of 7.4% has been reported.[5] Part of the improvement originated from the refinement of existing production techniques to optimize the active layer morphology.[6–8] The majority of the improvement, however, came from the development of low band gap polymers.[3,4,9–17] By decreasing the bandgap of the donor, the amount of absorbed photon flux increases due to an enhanced overlap with the solar spectrum. A lowering of the polymer band gap can either be achieved by a lowering of the lowest unoccupied molecular orbital (LUMO) or by a raise of the highest occupied molecular orbital (HOMO). The lowering of the LUMO is limited by the energy offset needed for electron transfer to the acceptor, typically 0.4 eV. A raise of the HOMO on the other hand will lead to a decrease of the open circuit voltage V_{oc}. A theoretical study by Koster et al.[18] showed that a decrease of the bandgap from 2.1 to 1.5 eV, by lowering the LUMO and keeping the HOMO in place, is expected to result in an increase in power conversion efficiency η from 3.5% to over 8%. This enhanced performance mainly originated from an increased short circuit current density J_{sc} due to an increased absorption. However, an increased absorption because of a better spectral overlap with the solar sprectrum also leads to an increased concentration of electrons and holes in the solar cells. This enhancement of the carrier density then gives rise to an increase of the bimolecular recombination, which is proportional to the product of the electron and hole density. Furthermore, the higher carrier densities make the solar cells also more sensitive for the built-up of space charge, caused by an imbalanced charge transport. Space charge built-up is also dependent on the absorption profiles in the solar cell, which were not included in these calculations. To obtain more insight in the operation of low band gap solar cells, combined optical and electrical modeling is required to address the role of the absorption profiles for wide and small bandgap polymer:fullerene solar cells as well as the role of unbalanced charge transport and enhanced recombination.

In this study, we simulate polymer:fullerene solar cells by systematically varying the polymer band gap. We compare wide and small bandgap polymer:fullerene bulk heterojunction solar cells with both unbalanced transport, where the hole mobility is an order of magnitude less than the electron mobility, and balanced transport with equal electron and hole mobilities. As a model system, we have chosen a blend of poly[2-methoxy-5-(3′,7′-dimethyloctyloxy)-*p*-phenylenevinylene] (MDMO-PPV) and 6,6-phenyl C_{61}-butyric acid methyl ester (PCBM) in a weight ratio of 1–4. To systematically simulate the effect of the band gap, the optical parameters of MDMO-PPV are red shifted in energy E from 0 to 0.8 eV in steps of 0.2 eV, such that the LUMO is lowered while the

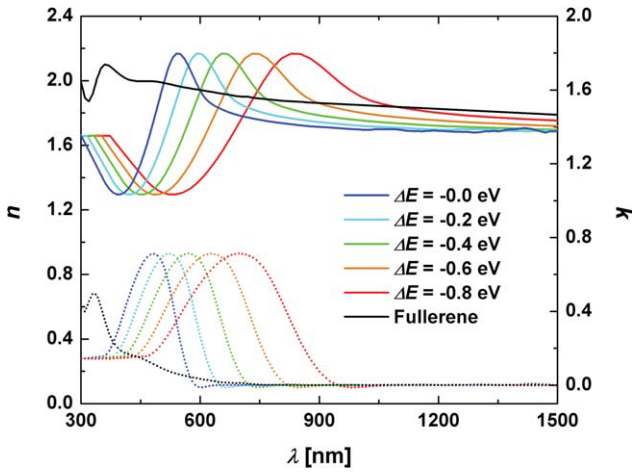

FIGURE 1 Optical parameters of PCBM and MDMO-PPV and four red-shifted variants as a function of wavelength λ.

HOMO is kept constant, to preserve the energy gap between the HOMO of the polymer and the LUMO of the PCBM and thus to preserve V_{oc}. The electron mobility μ_e of the PCBM is set to 2×10^{-7} cm^2/V s,[19] whereas the hole mobility μ_h is varied between 2×10^{-8} cm^2/V s[20] for the unequal mobility case and 2×10^{-7} cm^2/V s for balanced transport. All other optical and electrical parameters are equal to those of MDMO-PPV and are kept constant in the simulations. For a complete solar cell, we consider a glass substrate with a stack of thin layers on top of it: first 140 nm of indium tin oxide (ITO) as electrical contact, 50 nm of poly(3,4ethylenedioxythiophene)/poly(styrenesulphonic acid) (PEDOT:PSS) as anode, 10–500 nm of polymer:PCBM [1:4] as active layer, 0.5 nm of lithium fluoride (LiF) as electron injection layer, and 80 nm of aluminum (Al) as reflecting cathode. As optical model, we use the transfer matrix formalism as described by Pettersson et al.[21] The electrical modeling is based on a numerical device model as developed by Koster et al.[22] This model includes drift and diffusion of charge carriers, a temperature- and field-dependent generation rate of free carriers, bimolecular recombination, and the effect of space charge on the electric field in the device. The dissociation rate of bound pairs into free carriers is described by Onsager–Braun theory, and recombination of free carriers is assumed to be of the Langevin type. The optical model is used to calculate the photonic absorption rate profile inside the active layer using the AM 1.5 solar spectrum and the thickness and optical parameters of the various materials. Assuming 100% conversion efficiency from absorbed photons to excitons to bound electron–hole pairs, the electrical model is used to calculate the electrical behavior of the solar cell. As optical parameters, the complex refractive indices of the materials are used, where the values of PEDOT:PSS were reported by Pettersson et al.,[21] those of PCBM by Hoppe et al.,[23] and those of Al were taken from literature.[24] The values of the remaining materials, glass, ITO, MDMO-PPV, and LiF were determined with variable angle ellipsometry using a Woollam VASE ellipsometer. Figure 1 shows the n (solid lines) and k (dashed lines) as a function of λ from 300 to 1500 nm for PCBM, MDMO-PPV and four of its red-shifted variants with red shifts ΔE of 0.2–0.8 eV in steps of 0.2 eV. It should be noted that red shifting the optical parameters in equal energy parts translates into a larger shift in wavelength and a broadening of the spectral features, resulting in a higher photonic absorption rate. The optical properties of the polymer:PCBM blend are composed of 20% and 80% of the optical properties of the red-shifted MDMO-PPV polymer and PCBM.

Using the thicknesses and optical parameters of the materials in the transfer matrix formalism, the light intensity distribution inside the active layer can be calculated and with it the photon absorption rate as a function of position in the active layer. With the electrical parameters of the blend as described by Lenes et al.,[25] we calculate the short circuit current J_{sc}, the fill factor (FF), and η of the solar cells. Figure 2 shows J_{sc} as a function of active layer thickness L for a band gap shift ΔE from 0 to 0.8 eV in steps of 0.2 eV using an electron mobility μ_e of 2×10^{-7} m^2/V s and a hole mobility μ_h of 2×10^{-8} m^2/V s.[19,20] It is immediately clear that J_{sc} increases for increasing ΔE, due to a better overlap between absorption spectrum and solar spectrum. Typically, at the optimum layer thickness, J_{sc} increases from 44.8 to 82.7 A/m^2, representing a near doubling for a band gap shift from 2.4 to 1.6 eV. For very thin active layers (<50 nm), the increase in J_{sc} due to the band gap lowering increase is diminished due to destructive interference between incident and reflected light near the cathode, thereby decreasing the total light irradiance. The interference caused by the aluminum cathode also leads to an oscillatory behavior of the light absorption and thus J_{sc} on the active layer thickness. As photons with longer λ are absorbed for increasing ΔE, the interference patterns for those photons will have longer oscillatory periods for the internal absorption rate profiles and as

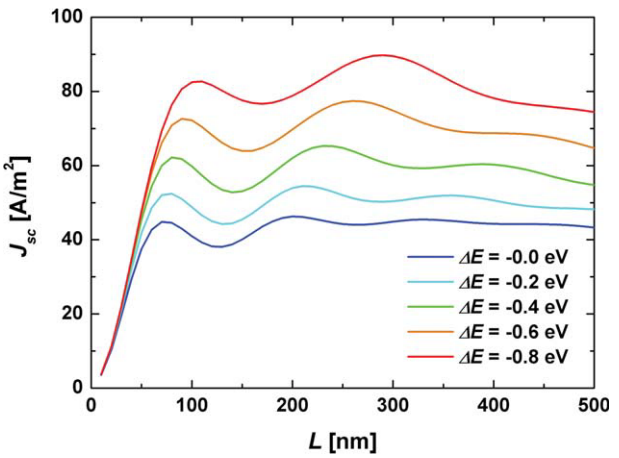

FIGURE 2 Short circuit current density J_{sc} as a function of active layer thickness L for red shift ΔE from 0 to 0.8 eV using $\mu_h = 2 \times 10^{-8}$ m^2/V s and $\mu_e = 2 \times 10^{-7}$ m^2/V s.

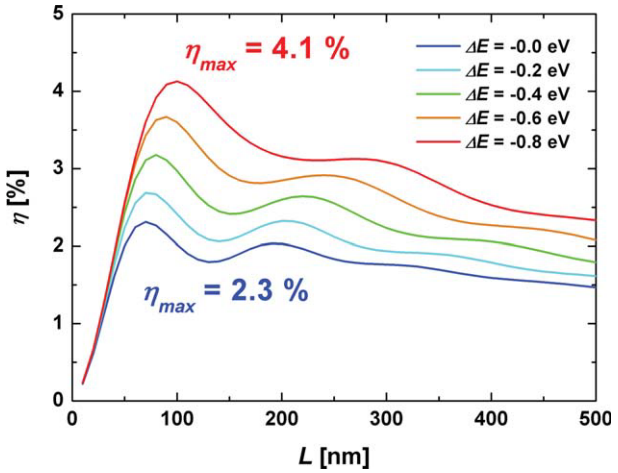

FIGURE 3 Efficiency η as a function of active layer thickness L for a red shift ΔE from 0 to 0.8 eV using μ_h of 2×10^{-8} m^2/V s and $\mu_e = 2 \times 10^{-7}$ m^2/V s.

a result the oscillatory features of J_{sc} shift to higher layer thickness, as observed in Figure 2. Quantitatively, for increasing ΔE from 0 to 0.8 eV, the optimum layer thickness increases from 70 to 110 nm.

As a next step, the efficiency η is calculated as a function of the red shifting of the polymer absorption spectrum. Figure 3 shows η as a function of L for ΔE from 0 to 0.8 eV in steps of 0.2 eV, using μ_e and μ_h of 2×10^{-7} and 2×10^{-8} m^2/V s, respectively. With increasing ΔE again the optimum layer thickness increases from 70 to 100 nm due to interference effect. The absolute value of η increases from 2.3% to 4.1%, respectively, which is a near doubling in η. A difference with J_{sc} is that η increases to a clear maximum and then decreases for increasing active layer thickness, indicating extra losses for increasingly thick layers.

For MDMO-PPV ($\Delta E = 0$), it was reported that the lowering of the efficiency with increasing thickness resulted from an increased recombination as the carriers have to travel a longer distance and an increase of the built-up of space charges because the transport is not completely balanced.[25] Furthermore, with increasing active layer thickness the electric fields are also reduced that lower the dissociation efficiency. However, for $\Delta E = 0.8$ eV the decrease of efficiency for thick devices is much stronger as compared to MDMO-PPV ($\Delta E = 0$). Both loss processes have a negative effect on the FF of the solar cell. The question now is whether the strong efficiency decrease for low band gap cells is due to a recombination increase because of the increased carrier densities or due to an enhanced built-up of space charges.

A way to evaluate the role of the various processes is to study the effect of an increase of the hole mobility μ_h to 2×10^{-7} m^2/V s, such that the transport is balanced. In this way, the effect of space charge formation will be eliminated. Figure 4a shows the FF as a function of L for ΔE from 0 to 0.8 eV in steps of 0.2 eV and μ_e and μ_h of 2×10^{-7} and 2×10^{-8} m^2/V s, respectively. As expected the FF decreases with increasing L, but for active layers thicker than 150 nm the curves for different band gap lowering ΔE start to diverge from each other. As a comparison, the decrease of FF with increasing L is shown in Figure 4b in case of balanced transport. In this case, the curves start diverging from 50 nm onward and show signs of oscillatory features. However, for all thickness the FF is substantially higher as compared to the unbalanced transport case. For example, around the second maximum (~250 nm) the FF in case of unbalanced transport is just below 40%, whereas for balanced transport it is still slightly above 50%. It should be noted that the imbalance in transport considered here is only one order of magnitude, which is typical

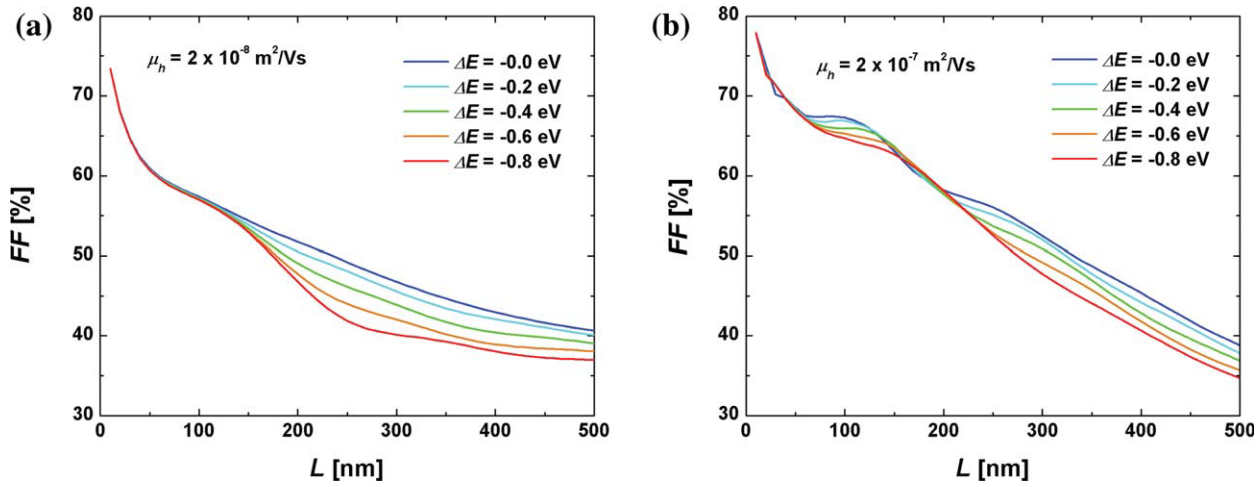

FIGURE 4 Fill factor (FF) as a function of active layer thickness L for red shift ΔE from 0 to 0.8 eV in steps of 0.2 eV and hole mobility μ_h of 2×10^{-8} m^2/V s (a) and 2×10^{-7} m^2/V s (b).

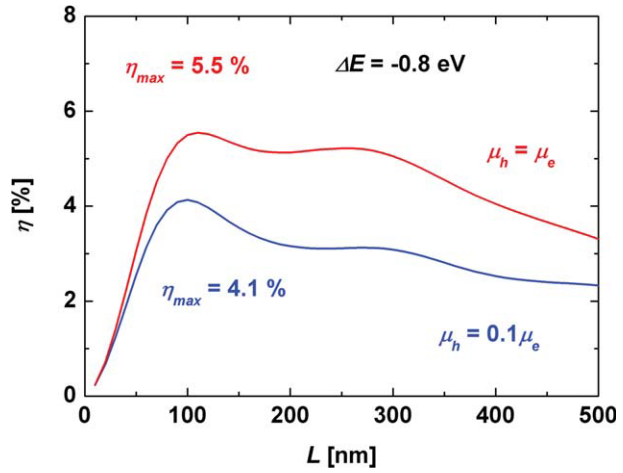

FIGURE 5 Efficiency η as a function of active layer thickness L for a red shift ΔE of 0.8 eV using μ_h of 2×10^{-8} m^2/V s and $\mu_h = 2 \times 10^{-7}$ m^2/V s, respectively. The electron mobility μ_e amounts to 2×10^{-7} m^2/V s.

for many polymer:fullerene cells. For a larger imbalance, the FF drops even more at these thicknesses. To evaluate the effect of charge balance, we compare in Figure 5 the efficiency η in case of balanced and unbalanced transport.

The balancing of the charge transport in this low band gap cell ($E_{gap} = 1.6$ eV) leads to a strong increase of the efficiency, from 4.1% to 5.5%. Furthermore, due to the balanced transport, the absorption increase for low bandgap cells is now also exploited in thicker cells (250 nm). The difference between the two interference maxima at 110 and 270 nm has almost disappeared. This result stresses the importance of balanced transport in low band gap polymer:fullerene solar cell. It should be noted that the recently reported values exceeding 7% make use of the fullerene [70]PCBM that complements the absorption of the low band gap polymer and therefore broadens the total absorption spectrum of the polymer:fullerene cell. With [60]PCBM, as used in our modeling, efficiencies of around 5% have been reported, in agreement with our results on low band gap cells with balanced charge transport.

In conclusion, the effect of band gap lowering of the polymer absorber in polymer:fullerene bulk heterojunction solar cells is modeled. For devices thinner than 50 nm the increase in J_{sc} due to the band gap lowering is limited due to interference effects. For 100 nm devices, a shift of 0.8 eV from 2.4 to 1.6 eV leads to an efficiency increase of only 2.3–4.1%. Due to space charge formation, a mobility difference of only one order of magnitude strongly limits the performance of low band gap devices (1.6 eV) thicker than 200 nm. As a result balancing of the charge transport is more crucial for low band gap solar cells: The increased absorption leads to higher carrier densities and therefore also to an enhanced space charge built-up.

REFERENCES AND NOTES

1 Shaheen, S. E.; Brabec, C. J.; Sariciftci, N. S.; Padinger, F.; Fromherz, T.; Hummelen, J. C. *Appl. Phys. Lett.* **2001,** *78*, 841–843.

2 Padinger, F.; Rittberger, R. S.; Sariciftci, N. S. *Adv. Funct. Mater.* **2003,** *13*, 85–88.

3 Peet, J.; Kim, J. Y.; Coates, N. E.; Ma, W. L.; Moses, D.; Heeger, A. J.; Bazan, G. C. *Nat. Mater.* **2007,** *6*, 497–500.

4 Mühlbacher, D.; Scharber, M.; Morana, M.; Zhu, Z.; Waller, D.; Gaudiana, R.; Brabec, C. *Adv. Mater.* **2006,** *18*, 2884–2887.

5 Liang, Y.; Xu, Z.; Xia, J.; Tsai, S. T.; Wu, Y.; Li, G.; Ray, C.; Yu, L. *Adv. Mater.* **2010,** *22*, E135–138.

6 Li, G.; Shrotriya, V.; Huang, J.; Yao, Y.; Moriarty, T.; Emery, K.; Yang, Y. *Nat. Mater.* **2005,** *4*, 864–868.

7 Ma, W.; Yang, C.; Gong, X.; Lee, K.; Heeger, A. J. *Adv. Funct. Mater.* **2005,** *15*, 1617–1622.

8 Mihailetchi, V. D.; Xie, H.; de Boer, B.; Koster, L. J. A.; Blom, P. W. M. *Adv. Funct. Mater.* **2006,** *16*, 699–708.

9 Dhanabalan, A.; van Duren, J. K. J.; van Hal, P. A.; van Dongen, J. L. J.; Janssen, R. A. J. *Adv. Funct. Mater.* **2001,** *11*, 255–262.

10 Wang, X.; Perzon, E.; Delgado, J. L.; De la Cruz, P. Zhang, F.; Langa, F.; Andersson, M. R.; Inganäs, O. *Appl. Phys. Lett.* **2004,** *85*, 5081–5083.

11 Zhang, F.; Mammo, W.; Andersson, L. M.; Admassie, S.; Andersson, M. R.; Inganäs, O. *Adv. Mater.* **2006,** *18*, 2169–2172.

12 Wienk, M. M.; Struijk, M. P.; Janssen, R. A. J. *Chem. Phys. Lett.* **2006,** *422*, 488–491.

13 Colladet, K.; Fourier, S.; Cleij, T. J.; Lutsen, L.; Gelan, J.; Vanderzande, D.; Nguyen, L. H.; Neugebauer, H.; Sariciftci, S.; Aguirre, A.; Janssen, G.; Goovaerts, E. *Macromolecules* **2007,** *40*, 65–72.

14 Perzon, E.; Zhang, F.; Andersson, M.; Mammo, W.; Inganäs, O.; Andersson, M. R. *Adv. Mater.* **2007,** *19*, 3308–3311.

15 Wienk, M. M.; Turbiez, M.; Gilot, J.; Janssen, R. A. J. *Adv. Mater.* **2008,** *20*, 2556–2559.

16 Hou, J.; Chen, H.-Y.; Zhang, S.; Li, G.; Yang, Y. *J. Am. Chem. Soc.* **2008,** *130*, 16144–16147.

17 Beaupre, S.; Boudreault, P. L. T.; Leclerc, M. *Adv. Mater.* **2010,** *22*, E6–E9.

18 Koster, L. J. A.; Mihailetchi, V. D.; Blom, P. W. M. *Appl. Phys. Lett.* **2006,** *88*, 093511-1–093511-3.

19 Mihailetchi, V. D.; van Duren, J. K. J.; Blom, P. W. M.; Hummelen, J. C.; Janssen, R. A. J.; Kroon, J. M.; Rispens, M. T.; Verhees, W. J. H.; Wienk, M. M. *Adv. Funct. Mater.* **2003,** *13*, 43–46.

20 Melzer, C.; Koop, E.; Mihailetchi, V. D.; Blom, P. W. M. *Adv. Funct. Mater.* **2004,** *14*, 865–870.

21 Pettersson, L. A. A.; Ghosh, S.; Inganäs, O. *Org. Electron.* **2002,** *3*, 143–148.

22 Koster, L. J. A.; Smits, E. C. P.; Mihailetchi, V. D.; Blom, P. W. M. *Phys. Rev. B* **2005,** *72*, 085205-1–085205-9.

23 Hoppe, H.; Sariciftci, N. S.; Meissner, D. *Mol. Cryst. Liq. Cryst. Sci. Technol. Sect. A* **2002,** *385*, 233–239.

24 Lide, D. R. Handbook of Chemistry and Physics; Chemical Rubber Company: Boca Raton, **1994.**

25 Lenes, M.; Koster, L. J. A.; Mihailetchi, V. D.; Blom, P. W. M. *Appl. Phys. Lett.* **2006,** *88*, 243502-1–243502-3.